Exact Landau Level Description of Geometry and Interaction in a Flatband

Jie Wang, Jennifer Cano, Andrew J. Millis, Zhao Liu, and Bo Yang

Phys. Rev. Lett. **127**, 246403 — Published 10 December 2021

DOI: 10.1103/PhysRevLett.127.246403

Exact Landau Level Description of Geometry and Interaction in a Flatband

Jie Wang,[1,*] Jennifer Cano,[1,2] Andrew J. Millis,[1,3] Zhao Liu,[4,†] and Bo Yang[5,6,‡]

[1] *Center for Computational Quantum Physics, Flatiron Institute, 162 5th Avenue, New York, NY 10010, USA*
[2] *Department of Physics and Astronomy, Stony Brook University, Stony Brook, New York 11974, USA*
[3] *Department of Physics, Columbia University, 538 W 120th Street, New York, New York 10027, USA*
[4] *Zhejiang Institute of Modern Physics, Zhejiang University, Hangzhou 310027, China*
[5] *Division of Physics and Applied Physics, Nanyang Technological University, 637371, Singapore*
[6] *Institute of High Performance Computing, A*STAR, 138632, Singapore*

Flatbands appear in many condensed matter systems, including the two dimensional electron gas in a high magnetic field, correlated materials and moiré heterostructures. They are characterized by intrinsic geometric properties such as the Berry curvature and Fubini-Study metric. The influence of the band geometry on electron-electron interaction is difficult to understand analytically because the geometry is in general nonuniform in momentum space. In this work, we study topological flatband of Chern number $\mathcal{C} = 1$ with a momentum-dependent but positive definite Berry curvature that fluctuates in sync with Fubini-Study metric. We derive an exact correspondence between such ideal flatbands and Landau levels and show that the band geometry fluctuation gives rise to a new type of interaction in the corresponding Landau levels that depends on the center-of-mass of two particles. We characterize such interactions by generalizing the usual Haldane pseudopotentials. This mapping gives exact zero-energy ground states for short-ranged repulsive generalized pseudopotentials in flatbands, in analogy to fractional quantum Hall systems. Driving the center-of-mass interactions beyond the repulsive regime leads to a dramatic reconstruction of the ground states towards gapless phases. The generalized pseudopotential could be a useful basis for future numerical studies.

The one-electron states in periodic solids are characterized both by their dispersion (variation of energy with crystal momentum) and by their band geometry, defined by the variation of the electronic wavefunction with crystal momentum. In a single-band system, the band geometry is defined by the quantum geometric tensor:

$$\mathcal{Q}^{ab}_{\boldsymbol{k}} = \langle D^a_{\boldsymbol{k}} u_{\boldsymbol{k}} | D^b_{\boldsymbol{k}} u_{\boldsymbol{k}} \rangle = g^{ab}_{\boldsymbol{k}} + \frac{i}{2}\epsilon^{ab}\Omega_{\boldsymbol{k}}, \tag{1}$$

where $u_{\boldsymbol{k}}(\boldsymbol{r}) = \langle \boldsymbol{r}|u_{\boldsymbol{k}}\rangle$ is the periodic part of the Bloch wavefunction $\psi_{\boldsymbol{k}}(\boldsymbol{r})$, $D^a_{\boldsymbol{k}}$ is the covariant derivative operator that adiabatically transports the wavefunction along the spatial direction $a = x, y$, and ϵ^{ab} is the antisymmetric tensor. Here the Berry curvature $\Omega_{\boldsymbol{k}}$, and the Fubini-Study metric (FSM) $g^{ab}_{\boldsymbol{k}}$, are respectively the imaginary and real part of the quantum geometric tensor [1].

The interplay of band geometry and dispersion has been elucidated on the single-particle level [2–4], where it leads to many interesting phenomena including the anomalous Hall effect [5, 6]. Recent experimental and theoretical interest on moiré materials has centered on the "flatband" situation [7–12], where the electron dispersion is small relative to interaction scales and the physics is controlled by electron-electron interactions. A growing body of evidence indicates that in flatband situations the band geometry plays a crucial role in determining the electron-electron interaction physics. For example, in the canonical lowest Landau level (LLL) problem of electrons with a continuous two dimensional translation invariance in a uniform perpendicular magnetic field, both $g^{ab}_{\boldsymbol{k}}$ and $\Omega_{\boldsymbol{k}}$ are $\boldsymbol{k}-$independent. This $\boldsymbol{k}-$independence enables detailed analytical understanding of the physics even in the presence of strong electron-electron interactions [13]. However, generically in periodic lattice systems the band geometry is highly nonuniform in momentum space, and while the interplay between band geometry and interactions has been numerically studied [14, 15] analytical understanding has been limited [16–26].

In this paper we take a step towards understanding the relation between band geometry and interaction physics. Our work is inspired by the chiral model of twisted bilayer graphene (cTBG) which at certain "magic" twist angles realizes exactly dispersionless bands [27]. The chiral model is understood as a kind of fixed point Hamiltonian [28] capturing the interacting physics of twisted bilayer graphene [29–31] and has the special property [17–19, 32] that while the band geometry is nonuniform, the FSM is related to the Berry curvature in the following way:

$$g^{ab}_{\boldsymbol{k}} = \frac{1}{2}\omega^{ab}\Omega_{\boldsymbol{k}}, \tag{2}$$

where ω^{ab} is a constant determinant one positive symmetric matrix.

Following Ref. (19), we define *ideal flatbands* as dispersionless Bloch bands with (i) a positive definite Berry curvature that (ii) fluctuates in sync with the FSM as in Eq. (2). We show that the ideal flatband assumptions (i) and (ii) fix the forms of single-particle wavefunctions in a topological flatband with Chern number $\mathcal{C} = 1$ (as occurs in cTBG), establishing an exact correspondence between an ideal flatband and the LLL. Using this correspondence we show that the electron-electron interaction in an ideal flatband with spatially fluctuating band geometry can

be exactly mapped to a center-of-mass (COM) dependent interaction in the LLL, which can be systematically characterized by the generalized COM pseudopotentials derived here. We show that the resulting interacting Hamiltonian possesses exact zero modes, corresponding to the previously discussed generalization of the Laughlin fractional quantum Hall states [32]; however, depending on the values of the COM interaction parameters, charge density wave states of lower energy may exist. In the last section of the supplementary material (SM), we derive further implications for superconductivity and the composite Fermi liquid phase in TBG flatbands.

Wavefunctions of $\mathcal{C}=1$ ideal flatbands.— Locally, such a flatband mimics a LL in $\boldsymbol{k}-$space: the quantum geometric tensor at every $\boldsymbol{k}$ point has a constant null vector $\mathcal{Q}^{ab}_{\boldsymbol{k}}\omega_b = 0$, which also determines $\omega^{ab} = \omega^a\omega^{b*} + \omega^{a*}\omega^b$ in Eq. (2). This uniform null vector defines the $\boldsymbol{k}-$space complex structure [33, 34] and gives the Bloch wavefunction a universal form [19]:

$$\psi_{\boldsymbol{k}}(\boldsymbol{r}) \sim \tilde{u}_k(\boldsymbol{r})\exp(i\boldsymbol{k}\cdot\boldsymbol{r}), \tag{3}$$

where the bolded $\boldsymbol{k}$ gives the momentum vector and unbolded $k \equiv \omega^a \boldsymbol{k}_a$ is a complex number. The cell-periodic function $\tilde{u}_k$ is holomorphic in k up to a normalization factor.

We define the $\boldsymbol{k}-$space boundary condition for the periodic part of the Bloch wavefunction:

$$\tilde{u}_{k+b}(\boldsymbol{r}) = e^{i\phi_{k,b}}e^{-i\boldsymbol{b}\cdot\boldsymbol{r}}\tilde{u}_k(\boldsymbol{r}). \tag{4}$$

The complex phase $\phi_{k,b}$ must be holomorphic in k because both $\tilde{u}_{k+b}$ and $\tilde{u}_k$ are. A non-zero Chern number requires that $\tilde{u}_k$, as a function of k, must have discontinuities in the Brillouin zone (BZ). Such discontinuities show up at the BZ boundary as non-zero $\phi_{k,b}$, in the bulk as wavefunction singularities, or both [35]. For a $\mathcal{C}=1$ ideal flatband, it is necessary to have non-zero $\phi_{k,b}$: in contrast, Ref. (19) assumed $\phi_{k,b}=0$ so discussions were limited to wavefunctions of $\mathcal{C}\geq 2$.

The boundary condition $\phi_{k,b}$ plays a crucial role in determining the wavefunction of the ideal band. Following Cauchy's argument principle, the BZ boundary integral $\frac{1}{2\pi i}\oint dk\ \partial_k \ln\tilde{u}_k(\boldsymbol{r})$ is an integer. We show in the SM that this integer is equal to the Chern number and can be written as [36]:

$$\mathcal{C} = -\frac{1}{2\pi}\left(\phi_{k_0+b_1,b_2} - \phi_{k_0,b_2} + \phi_{k_0,b_1} - \phi_{k_0+b_2,b_1}\right), \tag{5}$$

where, as illustrated in Fig. 1 (a), $b_{1,2}$ are primitive reciprocal lattice vectors and k_0 is the BZ origin. Insensitivity of the Chern number to the choice of k_0, combined with Eq. (5), forces $\phi_{k,b}$ to be a linear function of k. Since $\tilde{u}_k$ is holomorphic in k, it is uniquely determined by the boundary condition $\phi_{k,b}$, giving the bulk wavefunction:

$$\psi_{\boldsymbol{k}}(\boldsymbol{r}) = \mathcal{N}_{\boldsymbol{k}}\mathcal{B}(\boldsymbol{r})\Phi_{\boldsymbol{k}}(\boldsymbol{r}), \tag{6}$$

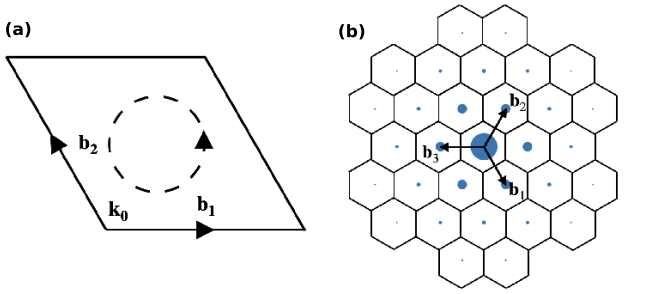

FIG. 1. (a) Geometry of the Brillouin zone: $\boldsymbol{k}_0$ is the origin, $\boldsymbol{b}_{1,2}$ are primitive reciprocal lattice vectors, and the dashed circle sketches the orientation of the Brillouin zone boundary integral used in Eq. (5). (b) Plot of reciprocal space of cTBG at the first magic angle with reciprocal lattice vectors used in the main text indicated, and the values of the Fourier modes $w_{\boldsymbol{b}}$ Eq. (9) indicated by the size of solid dots. We find the first two modes $w_{\boldsymbol{0}}=1$, $w_{\pm\boldsymbol{b}_{1,2,3}}=0.243$ dominate. The $w_{\boldsymbol{b}}$ determine the single-particle band geometry through Eq. (7) and Eq. (8), and the interaction model Eq. (10).

where $\mathcal{N}_{\boldsymbol{k}}$, $\mathcal{B}(\boldsymbol{r})$ and $\Phi_{\boldsymbol{k}}$ are the normalization factor, a $\boldsymbol{k}-$independent quasi-periodic function and the LLL wavefunction, respectively. Expressed in the symmetric gauge, $\Phi_{\boldsymbol{k}}(\boldsymbol{r}) = \sigma(z+ik)\exp\left(ik^*z\right)\exp\left(-\frac{1}{2}|z|^2 - \frac{1}{2}|k|^2\right)$ where $\sigma(z)$ is the modified Weierstrass sigma function [37–40] and $z \equiv \omega_a \boldsymbol{r}^a$ [41]. Generalizing to negative definite Berry curvature is straightforward. We leave more detailed discussions of the ideal flatband conditions, holomorphic wavefunction Eq. (3) and the uniqueness of our $\mathcal{C}=1$ model wavefunction Eq. (6) to SM [36].

Band geometry of ideal flatbands.— We now explicitly compute the band geometry of an ideal flatband using the model wavefunction Eq. (6). Exploiting the magnetic translation algebra of the LLL states, we find [36]:

$$\Omega_{\boldsymbol{k}} = 2\sqrt{\det g_{\boldsymbol{k}}} = -1 + \Delta_{\boldsymbol{k}}\log\mathcal{N}_{\boldsymbol{k}}, \tag{7}$$

where $\Delta_{\boldsymbol{k}}$ is the Laplace operator. Eq. (7) shows that the logarithm of the normalization factor $\mathcal{N}_{\boldsymbol{k}}$ is the $\boldsymbol{k}-$space Kähler potential [42], which controls the fluctuation of band geometry and can be explicitly calculated [36]:

$$\mathcal{N}_{\boldsymbol{k}}^{-2} = \sum_{\boldsymbol{b}} \eta_{\boldsymbol{b}} w_{\boldsymbol{b}} \exp\left(i\boldsymbol{k}\times\boldsymbol{b}\right)\exp\left(-\frac{1}{4}|\boldsymbol{b}|^2\right), \tag{8}$$

where $\eta_{\boldsymbol{b}}$=+1 if $\boldsymbol{b}/2$ is a reciprocal lattice vector and −1 otherwise, and $w_{\boldsymbol{b}}$ are the Fourier components of $|\mathcal{B}(\boldsymbol{r})|^2$:

$$|\mathcal{B}(\boldsymbol{r})|^2 = \sum_{\boldsymbol{b}} w_{\boldsymbol{b}}\exp(i\boldsymbol{b}\cdot\boldsymbol{r}), \tag{9}$$

where $\boldsymbol{b} = m_1\boldsymbol{b}_1 + m_2\boldsymbol{b}_2$, $m_{1,2}\in\mathbb{Z}$ is a reciprocal lattice vector. The band geometry is uniform if $w_{\boldsymbol{b}\neq\boldsymbol{0}}=0$.

Effective fractional quantum Hall model.—A consequence of the exact wavefunction in Eq. (6) is that the interacting physics in a $\mathcal{C}=1$ ideal flatband is described by

a FQH-type model with a new Umklapp interaction that breaks continuous translation symmetry. We demonstrate that this Umklapp interaction captures precisely the fluctuating band geometry of an ideal flatband.

We consider a generic translation invariant two-particle interaction $v(\boldsymbol{r}_1-\boldsymbol{r}_2)$. According to Eq. (6), projecting this interaction into an ideal flatband yields an effective FQH model with the interaction

$$\tilde{v}(\boldsymbol{r}_1,\boldsymbol{r}_2)=|\mathcal{B}(\boldsymbol{r}_1)\mathcal{B}(\boldsymbol{r}_2)|^2\cdot v(\boldsymbol{r}_1-\boldsymbol{r}_2), \tag{10}$$

$$\approx\sum_{\boldsymbol{q}}\left(\tilde{w}_0+\sum_{\boldsymbol{b}_i;j=1,2}(\tilde{w}_i e^{i\boldsymbol{b}_i\cdot\boldsymbol{r}_j}+h.c.)\right)v_{\boldsymbol{q}}e^{i\boldsymbol{q}(\boldsymbol{r}_1-\boldsymbol{r}_2)}, \tag{11}$$

projected to the LLL, where the normalization factors have been dropped due to their weak $\boldsymbol{k}-$dependence according to Eq. (8). The factor $|\mathcal{B}(\boldsymbol{r})|^2$ reduces the continuous translation symmetry of $v(\boldsymbol{r}_1-\boldsymbol{r}_2)$ to the discrete lattice translation symmetry of $\tilde{v}(\boldsymbol{r}_1,\boldsymbol{r}_2)$. Such a symmetry reduction manifests itself as the inclusion of the "Umklapp" terms [43] that scatter electrons across the BZ which distinguish Eq. (10) from the usual FQH models.

The effective FQH model Eq. (10) can be simplified by retaining only the leading Umklapp processes that scatter electrons by the shortest distance in $\boldsymbol{k}-$space, because other Umklapp terms are suppressed after the LLL projection. This leads to Eq. (11) where the Umklapp interaction parameters $\tilde{w}_{0,1}$ can be easily derived from the Fourier modes $w_{\boldsymbol{b}}$ [44]. To verify the validity of this approximation, we consider electrons at 1/3 filling in the spin-valley polarized topological flatband of cTBG at the first magic angle. In this case, $\mathcal{B}(\boldsymbol{r})$ is a two-component layer spinor $(i\mathcal{G}(\boldsymbol{r}),\mathcal{G}(-\boldsymbol{r}))^T$ [45]. The leading Umklapp processes scatter electrons by $\boldsymbol{b}_{1,2,3}$, shown in Fig. 1 with the same real amplitude $\tilde{w}_1$ due to the $\mathcal{C}_3$ and exact intra-valley inversion symmetries [45]. In Fig. 1 (b), we plot the wavefunction's Fourier mode $w_{\boldsymbol{b}}$ of $|\mathcal{G}(\boldsymbol{r})|^2+|\mathcal{G}(-\boldsymbol{r})|^2$ and find $w_{\boldsymbol{0}}, w_{\boldsymbol{b}_1}$ dominate, which determines the parameters in Eq. (11) to be $(\tilde{w}_0,\tilde{w}_1)=(1.35,0.3)$ [44]. We assume electrons interact via a layer-isotropic v_1 Haldane pseudopotential $v(\boldsymbol{r}_1-\boldsymbol{r}_2)=\delta''(\boldsymbol{r}_1-\boldsymbol{r}_2)$ [13]. Remarkably, the entire low-energy spectrum of the cTBG model on the torus (blue dots in Fig. 2), including both the three-fold degenerate ground states at zero energy and the gapped low-lying magneto-roton mode [46, 47], is well reproduced by the effective FQH model Eq. (11) with $\tilde{w}_0$ and $\tilde{w}_1$ (red crosses in Fig. 2 a). However, if we assume a uniform band geometry by setting $\tilde{w}_1=0$, the obtained spectrum (red crosses in Fig. 2 b) shows significant deviations from the cTBG spectrum although the ground states stay at zero energy. This indicates our effective FQH model with nonzero $\tilde{w}_1$ indeed captures the spatially fluctuating band geometry of cTBG flatband.

Center-of-mass pseudopotentials.—The exact many-body zero modes observed above are the generalized-Laughlin states given in Ref. (32), written here as $\Phi=\left(\prod_{i=1}^{N}\mathcal{B}(\boldsymbol{r}_i)\right)\Psi$, where Ψ is the usual LLL Laughlin wavefunction. We now extend Haldane's pseudopotentials to capture the COM interactions. This allows us to systematically study how interactions can stabilize FQH states subject to nonuniform band geometry. We start by rewriting Eq. (10) as follows:

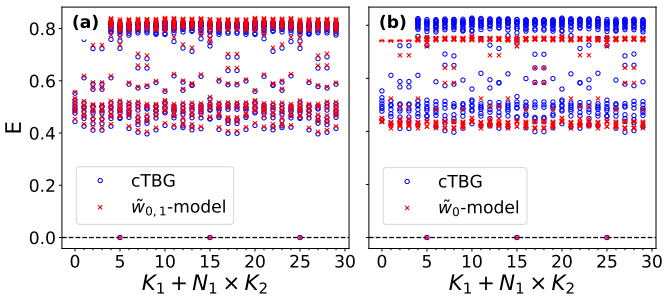

FIG. 2. Exact diagonalization of $N=10$ particles in a TBG lattice of $(N_1,N_2)=(5,6)$ unit cells on the torus geometry, where $N_{1,2}$ are the number of unit cells along each primitive lattice direction. Many-body momenta $K_1\in[0,N_1-1]$, $K_2\in[0,N_2-1]$ are integers labeling each energy level [48, 49]. Blue circles are energies of cTBG with relative interaction v_1, and are the same in both panels. Red crosses are energies of the FQH model Eq. (11) with (a) $(\tilde{w}_0,\tilde{w}_1)=(1.35,0.3)$ and (b) $(\tilde{w}_0,\tilde{w}_1)=(1.35,0)$. Normalization factors Eq. (8) are taken into account in numerical calculations. Including $\tilde{w}_1$ in (a) closely reproduces the low-energy details of the cTBG spectrum. Three exact zero-modes are visible in both cTBG and the FQH models.

$$\tilde{v}(\boldsymbol{r}_1,\boldsymbol{r}_2)=\int d\boldsymbol{q}_+^2 d\boldsymbol{q}_-^2\,\tilde{v}_{\boldsymbol{q}_+,\boldsymbol{q}_-}e^{i(\boldsymbol{q}_+\cdot\boldsymbol{R}^+ +\boldsymbol{q}_-\cdot\boldsymbol{R}^-)}, \tag{12}$$

$$=\sum_{M,m}c_{M,m}\hat{P}_M^+\hat{P}_m^-, \tag{13}$$

where $\boldsymbol{R}^+$ and $\boldsymbol{R}^-$ are the LLL projected COM and relative coordinates of two particles. A generic two-particle interaction can be expressed in terms of its COM/relative translational momentum $\boldsymbol{q}_+/\boldsymbol{q}_-$ as in Eq. (12). For simplicity, we assume rotational symmetry, so that we can define projectors $\hat{P}_m^{\pm}\equiv 2\int\frac{d^2\boldsymbol{q}}{(2\pi)^2}L_m(\boldsymbol{q}^2)e^{-\boldsymbol{q}^2/2}e^{i\boldsymbol{q}\cdot\boldsymbol{R}^{\pm}}$ which project the particle pair into its COM and relative angular momentum sectors respectively. The interacting Hamiltonian $\tilde{v}(\boldsymbol{r}_1,\boldsymbol{r}_2)$ can then be written as Eq. (13), where $c_{M,m}=\int d\boldsymbol{q}_+^2 d\boldsymbol{q}_-^2\,\tilde{v}_{\boldsymbol{q}_+,\boldsymbol{q}_-}L_M(\boldsymbol{q}_+^2)L_m(\boldsymbol{q}_-^2)$ is the generalized pseudopotential coefficient and L_m is the Laguerre polynomial. The $c_{M,m}$ can be extracted from the energy spectrum of two interacting particles [50, 51].

The key insight here is that if $c_{M,1}>0$ and $c_{M,m>1}=0$, the generalized Laughlin state Φ has exactly zero energy, no matter how $c_{M,1}$ depends on the COM angular momentum M. We can thus construct a family of many-body states that are topologically equivalent to the Laughlin state, where the usual Laughlin state cor-

responds to the special case where $c_{M,1}$ is independent of M. Generalization to periodic lattice systems without rotational invariance is straightforward with generalized Laguerre polynomials [52, 53]. We emphasis that the statement is unchanged even if rotational invariance is broken: Eqs. (10) and (11) exhibit three-fold exact zero-modes at one-third filling for arbitrary orders of Umklapp scatterings of arbitrary strengths even with the $\boldsymbol{k}-$dependent normalization factors, as long as the relative interaction is the v_1 Haldane pseudopotential [36].

Center-of-mass interaction induced transitions.—We now examine how the ground state and low energy physics of the effective FQH model in Eq. (11) evolves with $\tilde{w}_1/\tilde{w}_0$. We note that $\tilde{w}_1/\tilde{w}_0$ is constrained by band geometry; for example on a rectangular lattice with the v_1 interaction $|\tilde{w}_1/\tilde{w}_0| \leq 0.25$ [44]. However, sign changes in Ω_k or additional structure in the interaction may widen the allowed range. In Fig. 3, we plot the ground state energies in unit of $\tilde{w}_0$ on the rectangular lattice as a function of $\tilde{w}_1/\tilde{w}_0$. We find that the ground state is the zero-energy generalized Laughlin state for small $|\tilde{w}_1/\tilde{w}_0|$. However for large enough $|\tilde{w}_1/\tilde{w}_0|$, the ground state energy becomes negative and the zero-energy generalized Laughlin state is an excited state. The occurrence of the negative-energy ground states can also be seen from the COM pseudopotentials plotted in Fig. 3 (b), where regions with negative values are shown.

To further understand the negative-energy ground states of the generalized FQH model, we compute the guiding-center structure factor $S(\boldsymbol{q}) \equiv (\langle\rho(\boldsymbol{q})\rho(-\boldsymbol{q})\rangle - \langle\rho(\boldsymbol{q})\rangle\langle\rho(-\boldsymbol{q})\rangle)/(N_1N_2)$, at $\tilde{w}_1/\tilde{w}_0 = 0.3$ (before transition) and 0.5 (after transition) for $N = 12$ electrons in the $(N_1, N_2) = (6, 6)$ lattice. The $S(\boldsymbol{q})$ measures the density-density correlations of guiding centers and $\rho(\boldsymbol{q}) \equiv \exp(i\boldsymbol{q}\cdot\boldsymbol{R})$ is the LLL-projected density operator. At $\tilde{w}_1/\tilde{w}_0 = 0.3$, the ground states are in the many-body momentum $K = (0, 0)$ sector with exact zero energy. The corresponding structure factor has continuous peaks consistent with the incompressible Laughlin liquid. At $\tilde{w}_1/\tilde{w}_0 = 0.5$, the ground state is still in the $K = (0, 0)$ sector, with nearby low-lying states at $\pm K_{\boldsymbol{q}}$ and $\pm\mathcal{C}_4 K_{\boldsymbol{q}}$ where $K_{\boldsymbol{q}} = (3, 0)$ and $\mathcal{C}_4$ is the rotation by $\pi/2$. Remarkably, $S(\boldsymbol{q})$ has discretized peaks exactly at $\pm K_{\boldsymbol{q}}$ and $\pm\mathcal{C}_4 K_{\boldsymbol{q}}$. That the structure factor peak occurs exactly at momenta corresponding to low-energy excitations strongly suggests a gapless charge density wave (CDW) at $\tilde{w}_1/\tilde{w}_0 = 0.5$ [54]. The gapless CDW is analogous to the stripe phase and Wigner crystal reported in usual FQH systems at low filling factors. However in contrast to the usual FQH system, here the transition at a fixed filling factor 1/3 is driven entirely by the band geometry and the transition occurs as a level crossing in Laughlin states' momentum sector $K = (0, 0)$.

Discussion.—We have studied interacting physics in ideal flatbands with inhomogeneous but constrained band geometries. Employing the exact correspondence

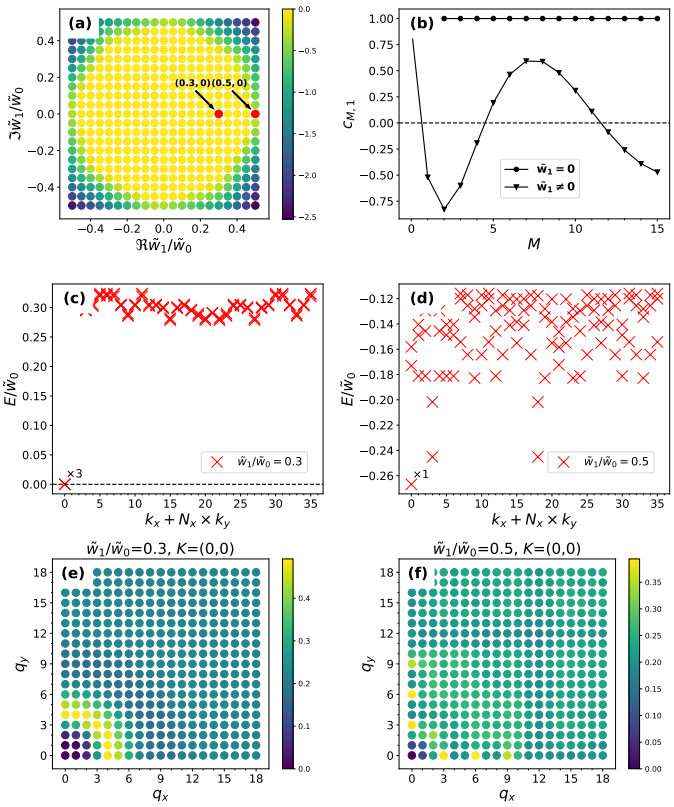

FIG. 3. Center-of-mass interaction induced transitions. (a): Ground-state energies of the model in Eq. (11) as a function of $\tilde{w}_1/\tilde{w}_0$. Three fold exact zero-modes are present for all values of $\tilde{w}_1/\tilde{w}_0$ (which remains true if $\tilde{w}_n$ is included to any order n). The appearance of negative-energy ground states is possible due to the negative value of the center-of-mass pseudopotential plotted in (b). Figures (c,d) and (e,f) are respectively the spectrum and the ground-state guiding-center structure factor $S(\boldsymbol{q})$ for the two marked data points in (a) that represent typical phases before and after the transition. (c) and (e): at $\tilde{w}_1/\tilde{w}_0 = 0.3$, the three-fold degenerate zero-energy ground states, finite gap and continuous peak in $S(\boldsymbol{q})$ are consistent with the Laughlin state. (d) and (f): at $\tilde{w}_1/\tilde{w}_0 = 0.5$, the single negative-energy ground state, small excitation gap and discretized peaks in $S(\boldsymbol{q})$ suggest a CDW phase. Plots are for a rectangular lattice on the torus, with $\boldsymbol{b}_1 \cdot \boldsymbol{b}_2 = 0$ and $|\boldsymbol{b}_1| = |\boldsymbol{b}_2|$. The system sizes are $N = 8$, $(N_1, N_2) = (4, 6)$ in (a), and $N = 12$, $(N_1, N_2) = (6, 6)$ in (c-f).

to LLLs, we mapped the inhomogeneous band geometry in a flatband to a COM interaction in the LLL. Remarkably, as shown in FIG. 3 (b), the COM interaction generically has attractive components, driving a phase transition [55] from the Laughlin state to gapless states.

The attractive interaction induced by band geometry implies new physics; applying COM pseudopotentials enables systematic studies of various instabilities which will be immediately useful for a wide range of applications [29–31, 56–70]. We conclude with two more examples. Recently, skyrmion pairing has been proposed to explain the superconductivity in TBG [71], which was sub-

sequently numerically tested in a simplified LLL based model with flat band geometries [72]. It is thus important to examine how inhomogeneous band geometry influences superconductivity. In the last section of the SM, we find the COM interaction induced by band geometry in time-reversal invariant TBG flatbands exhibits attractive components, which would favor superconductivity when its spatial pattern matches the superconducting order parameter. A thorough understanding requires extensive numerical studies that we leave for future work. The COM interaction is not only a novel concept but also a useful numerical tool, which we demonstrate through the second example by studying the stability of composite Fermi liquid (CFL) in the spin-valley polarized cTBG flatband. By continuously interpolating between the LLL and cTBG flatbands using the ideal flatband theory, we find that CFLs remain ground states of cTBG without signatures of phase transitions. Generalizations to higher Chern number and Hofstadter-type models are interesting future directions [73–77].

Acknowledgements.— The Flatiron Institute is a division of the Simons Foundation. J. W. acknowledges Martin Claassen, Debanjan Chowdhury and Kun Yang for useful discussions. J. C. acknowledges the support of the Air Force Office of Scientific Research under Grant No. FA9550-20-1-0260. A. J. M. is supported in part by Programmable Quantum Materials, an Energy Frontier Research Center funded by the U.S. Department of Energy (DOE), Office of Science, Basic Energy Sciences (BES), under award DE-SC0019443. Z. L. is supported by the National Key Research and Development Program of China through Grant No. 2020YFA0309200. B. Y. is supported by the Singapore National Research Foundation (NRF) under NRF fellowship award NRF-NRFF12-2020-0005.

* jiewang@flatironinstitute.org
† zhaol@zju.edu.cn
‡ yang.bo@ntu.edu.sg

[1] We use the convention that Berry connection and Berry curvature are $\boldsymbol{A}^a_{\boldsymbol{k}} = -i\langle u_{\boldsymbol{k}}|\partial^a_{\boldsymbol{k}} u_{\boldsymbol{k}}\rangle$ and $\Omega_{\boldsymbol{k}} = \epsilon_{ab}\partial^a_{\boldsymbol{k}}\boldsymbol{A}^b_{\boldsymbol{k}}$ respectively, which differs from the usual convention by a minus sign, but gives us $\boldsymbol{k}-$space holomorphic wavefunctions with positive Berry curvature. This sign convention was used, for instance, in Ref. (6).
[2] D. Vanderbilt, *Berry Phases in Electronic Structure Theory: Electric Polarization, Orbital Magnetization and Topological Insulators* (Cambridge University Press, 2018).
[3] D. Xiao, M.-C. Chang, and Q. Niu, Rev. Mod. Phys. **82**, 1959 (2010).
[4] S. Peotta and P. Törmä, Nature Communications **6**, 8944 (2015).
[5] N. Nagaosa, J. Sinova, S. Onoda, A. H. MacDonald, and N. P. Ong, Rev. Mod. Phys. **82**, 1539 (2010).
[6] F. D. M. Haldane, Phys. Rev. Lett. **93**, 206602 (2004).
[7] R. Bistritzer and A. H. MacDonald, Proceedings of the National Academy of Sciences **108**, 12233 (2011), https://www.pnas.org/content/108/30/12233.full.pdf.
[8] J. M. B. Lopes dos Santos, N. M. R. Peres, and A. H. Castro Neto, Phys. Rev. B **86**, 155449 (2012).
[9] Y. Cao, V. Fatemi, S. Fang, K. Watanabe, T. Taniguchi, E. Kaxiras, and P. Jarillo-Herrero, Nature **556**, 43 (2018).
[10] Y. Cao, V. Fatemi, A. Demir, S. Fang, S. L. Tomarken, J. Y. Luo, J. D. Sanchez-Yamagishi, K. Watanabe, T. Taniguchi, E. Kaxiras, R. C. Ashoori, and P. Jarillo-Herrero, Nature **556**, 80 (2018).
[11] A. L. Sharpe, E. J. Fox, A. W. Barnard, J. Finney, K. Watanabe, T. Taniguchi, M. A. Kastner, and D. Goldhaber-Gordon, Science **365**, 605 (2019).
[12] M. Serlin, C. L. Tschirhart, H. Polshyn, Y. Zhang, J. Zhu, K. Watanabe, T. Taniguchi, L. Balents, and A. F. Young, Science **367**, 900 (2020).
[13] F. D. M. Haldane, Phys. Rev. Lett. **51**, 605 (1983).
[14] N. Regnault and B. A. Bernevig, Phys. Rev. X **1**, 021014 (2011).
[15] E. J. BERGHOLTZ and Z. LIU, International Journal of Modern Physics B **27**, 1330017 (2013), https://doi.org/10.1142/S021797921330017X.
[16] S. A. Parameswaran, R. Roy, and S. L. Sondhi, Comptes Rendus Physique **14**, 816 (2013), topological insulators / Isolants topologiques.
[17] R. Roy, Phys. Rev. B **90**, 165139 (2014).
[18] T. S. Jackson, G. Möller, and R. Roy, Nature Communications **6**, 8629 (2015).
[19] M. Claassen, C. H. Lee, R. Thomale, X.-L. Qi, and T. P. Devereaux, Phys. Rev. Lett. **114**, 236802 (2015).
[20] Y.-L. Wu, N. Regnault, and B. A. Bernevig, Phys. Rev. Lett. **110**, 106802 (2013).
[21] C. H. Lee, R. Thomale, and X.-L. Qi, Phys. Rev. B **88**, 035101 (2013).
[22] C. H. Lee and X.-L. Qi, Phys. Rev. B **90**, 085103 (2014).
[23] C. H. Lee, M. Claassen, and R. Thomale, Phys. Rev. B **96**, 165150 (2017).
[24] C. H. Lee, Z. Papić, and R. Thomale, Phys. Rev. X **5**, 041003 (2015).
[25] S. D. Geraedts, J. Wang, E. H. Rezayi, and F. D. M. Haldane, Phys. Rev. Lett. **121**, 147202 (2018).
[26] J. Wang, Phys. Rev. Lett. **122**, 257203 (2019).
[27] G. Tarnopolsky, A. J. Kruchkov, and A. Vishwanath, Phys. Rev. Lett. **122**, 106405 (2019).
[28] O. Vafek and J. Kang, Phys. Rev. Lett. **125**, 257602 (2020).
[29] N. Bultinck, E. Khalaf, S. Liu, S. Chatterjee, A. Vishwanath, and M. P. Zaletel, Phys. Rev. X **10**, 031034 (2020).
[30] B. Lian, Z.-D. Song, N. Regnault, D. K. Efetov, A. Yazdani, and B. A. Bernevig, "Tbg iv: Exact insulator ground states and phase diagram of twisted bilayer graphene," (2020), arXiv:2009.13530 [cond-mat.str-el].
[31] B. A. Bernevig, B. Lian, A. Cowsik, F. Xie, N. Regnault, and Z.-D. Song, "Tbg v: Exact analytic many-body excitations in twisted bilayer graphene coulomb hamiltonians: Charge gap, goldstone modes and absence of cooper pairing," (2020), arXiv:2009.14200 [cond-mat.str-el].
[32] P. J. Ledwith, G. Tarnopolsky, E. Khalaf, and A. Vishwanath, Phys. Rev. Research **2**, 023237 (2020).
[33] T. Ozawa and B. Mera, arXiv e-prints , arXiv:2103.11582

(2021), arXiv:2103.11582 [cond-mat.mes-hall].
[34] B. Mera and T. Ozawa, arXiv e-prints , arXiv:2103.11583 (2021), arXiv:2103.11583 [cond-mat.mes-hall].
[35] D. J. Thouless, Journal of Physics C: Solid State Physics **17**, L325 (1984).
[36] SM includes detailed discussions on: model wavefunctions, ideal conditions, interacting models, pseudopotentials and numerical details.
[37] F. D. M. Haldane, Journal of Mathematical Physics **59**, 071901 (2018), https://doi.org/10.1063/1.5042618.
[38] J. Wang, S. D. Geraedts, E. H. Rezayi, and F. D. M. Haldane, Phys. Rev. B **99**, 125123 (2019).
[39] R. Ferrari, Phys. Rev. B **42**, 4598 (1990).
[40] R. FERRARI, International Journal of Modern Physics B **09**, 3333 (1995), https://doi.org/10.1142/S0217979295001300.
[41] Compared to the commonly used Jacobi θ function representation (Landau gauge), the σ function representation (symmetric gauge) has the advantage of labeling LLL states by two quantum numbers $\boldsymbol{k} = (k_1, k_2)$ in the same way of labeling Bloch states in solids. Different representations are related by gauge transformations discussed in SM.
[42] M. R. Douglas and S. Klevtsov, Communications in Mathematical Physics **293**, 205 (2009).
[43] We use "Umklapp interaction" and "COM interaction" inter-changeably.
[44] The COM interaction parameters are: $\tilde{w}_0 = w_{\mathbf{0}}^2 + 4|w_{\boldsymbol{b}_1}|^2$, $\tilde{w}_1 = w_{\mathbf{0}} w_{\boldsymbol{b}_1}$ on square lattice; $\tilde{w}_0 = w_{\mathbf{0}}^2 + 6|w_{\boldsymbol{b}_1}|^2$, $\tilde{w}_1 = w_{\mathbf{0}} w_{\boldsymbol{b}_1} + w_{\boldsymbol{b}_1}^{*2}$ on triangular lattice. See SM for details.
[45] J. Wang, Y. Zheng, A. J. Millis, and J. Cano, arXiv e-prints , arXiv:2010.03589 (2020), arXiv:2010.03589 [cond-mat.mes-hall].
[46] S. M. Girvin, A. H. MacDonald, and P. M. Platzman, Phys. Rev. Lett. **54**, 581 (1985).
[47] C. Repellin, T. Neupert, Z. Papić, and N. Regnault, Phys. Rev. B **90**, 045114 (2014).
[48] F. D. M. Haldane and E. H. Rezayi, Phys. Rev. B **31**, 2529 (1985).
[49] F. D. M. Haldane, Phys. Rev. Lett. **55**, 2095 (1985).
[50] Z. Liu, E. J. Bergholtz, and E. Kapit, Phys. Rev. B **88**, 205101 (2013).
[51] A. M. Läuchli, Z. Liu, E. J. Bergholtz, and R. Moessner, Phys. Rev. Lett. **111**, 126802 (2013).
[52] B. Yang, Z.-X. Hu, C. H. Lee, and Z. Papić, Phys. Rev. Lett. **118**, 146403 (2017).
[53] B. Yang, C. H. Lee, C. Zhang, and Z.-X. Hu, Phys. Rev. B **96**, 195140 (2017).
[54] K. Yang, F. D. M. Haldane, and E. H. Rezayi, Phys. Rev. B **64**, 081301 (2001).
[55] P. Wilhelm, T. C. Lang, and A. M. Läuchli, Phys. Rev. B **103**, 125406 (2021).
[56] J. Liu, J. Liu, and X. Dai, Phys. Rev. B **99**, 155415 (2019).
[57] F. K. Popov and A. Milekhin, Phys. Rev. B **103**, 155150 (2021).
[58] N. Bultinck, S. Chatterjee, and M. P. Zaletel, Phys. Rev. Lett. **124**, 166601 (2020).
[59] A. Abouelkomsan, Z. Liu, and E. J. Bergholtz, Phys. Rev. Lett. **124**, 106803 (2020).
[60] C. Repellin and T. Senthil, Phys. Rev. Research **2**, 023238 (2020).
[61] C. Repellin, Z. Dong, Y.-H. Zhang, and T. Senthil, Phys. Rev. Lett. **124**, 187601 (2020).
[62] Y.-H. Zhang, D. Mao, Y. Cao, P. Jarillo-Herrero, and T. Senthil, Phys. Rev. B **99**, 075127 (2019).
[63] F. Xie, A. Cowsik, Z. Son, B. Lian, B. A. Bernevig, and N. Regnault, "Tbg vi: An exact diagonalization study of twisted bilayer graphene at non-zero integer fillings," (2020), arXiv:2010.00588 [cond-mat.str-el].
[64] Y. H. Kwan, G. Wagner, T. Soejima, M. P. Zaletel, S. H. Simon, S. A. Parameswaran, and N. Bultinck, arXiv e-prints , arXiv:2105.05857 (2021), arXiv:2105.05857 [cond-mat.str-el].
[65] N. Stefanidis and I. Sodemann, Phys. Rev. B **102**, 035158 (2020).
[66] Y. H. Kwan, Y. Hu, S. H. Simon, and S. A. Parameswaran, Phys. Rev. Lett. **126**, 137601 (2021).
[67] Y. H. Kwan, Y. Hu, S. H. Simon, and S. A. Parameswaran, arXiv e-prints , arXiv:2003.11559 (2020), arXiv:2003.11559 [cond-mat.str-el].
[68] Y. Xu, S. Liu, D. A. Rhodes, K. Watanabe, T. Taniguchi, J. Hone, V. Elser, K. F. Mak, and J. Shan, Nature **587**, 214 (2020).
[69] E. C. Regan, D. Wang, C. Jin, M. I. Bakti Utama, B. Gao, X. Wei, S. Zhao, W. Zhao, Z. Zhang, K. Yumigeta, M. Blei, J. D. Carlström, K. Watanabe, T. Taniguchi, S. Tongay, M. Crommie, A. Zettl, and F. Wang, Nature **579**, 359 (2020).
[70] H. Polshyn, Y. Zhang, M. A. Kumar, T. Soejima, P. Ledwith, K. Watanabe, T. Taniguchi, A. Vishwanath, M. P. Zaletel, and A. F. Young, arXiv e-prints , arXiv:2104.01178 (2021), arXiv:2104.01178 [cond-mat.str-el].
[71] E. Khalaf, S. Chatterjee, N. Bultinck, M. P. Zaletel, and A. Vishwanath, arXiv e-prints , arXiv:2004.00638 (2020), arXiv:2004.00638 [cond-mat.str-el].
[72] S. Chatterjee, M. Ippoliti, and M. P. Zaletel, arXiv e-prints , arXiv:2010.01144 (2020), arXiv:2010.01144 [cond-mat.str-el].
[73] E. Kapit and E. Mueller, Phys. Rev. Lett. **105**, 215303 (2010).
[74] Z. Liu, A. Abouelkomsan, and E. J. Bergholtz, Phys. Rev. Lett. **126**, 026801 (2021).
[75] B. Andrews and A. Soluyanov, Phys. Rev. B **101**, 235312 (2020).
[76] B. Andrews and G. Möller, Phys. Rev. B **97**, 035159 (2018).
[77] B. Andrews, M. Mohan, and T. Neupert, Phys. Rev. B **103**, 075132 (2021).